Brittle-to-ductile transition in ultrathin Ta/Cu film systems

Patric A. Gruber[a)]
Universität Stuttgart, Institute of Physical Metallurgy, D-70569 Stuttgart, Germany

Eduard Arzt
INM Leibniz Institute for New Materials, D-66123 Saarbrücken, Germany

Ralph Spolenak[b)]
Laboratory for Nanometallurgy, Department of Materials, ETH Zurich, 8093 Zurich, Switzerland

(Received 20 May 2008; accepted 23 March 2009)

Current semiconductor technology demands the use of compliant substrates for flexible integrated circuits. However, the maximum total strain of such devices is often limited by the extensibility of the metallic components. Although cracking in thin films is extensively studied theoretically, little experimental work has been carried out thus far. Here, we present a systematic study of the cracking behavior of 34 to 506 nm thick Cu films on polyimide with 3.5 to 19 nm-thick Ta interlayers. The film systems have been investigated by a synchrotron-based tensile testing technique and in situ tensile tests in a scanning electron microscope. By relating the energy release during cracking obtained from the stress-strain curves to the crack area, the fracture toughness of the Cu films can be obtained. It increases with Cu film thickness and decreases with increasing Ta film thickness. Films thinner than 70 nm exhibit brittle fracture, indicating an increasing inherent brittleness of the Cu films.

I. INTRODUCTION

Flexible electronics have gained widespread interest for numerous applications. Among these are flexible displays,[1,2] wearable electronics,[3,4] electronic skins,[5] and flexible microelectrode arrays (MEAs) usable for in vivo biological applications such as retina implants.[6,7] The functional parts of these devices comprise stiff materials (e.g., metals, transparent conductors, and amorphous silicon) deposited on compliant substrates (e.g., polyimide or silicone). When stretched or bent during use, the compliant substrate usually deforms elastically. Brittle coatings or conducting wires may crack or delaminate as a consequence. Mechanical failure is one of the most critical issues in the development of flexible and stretchable electronics.

On the other hand, the measurement of fracture toughness of thin films is difficult because of small testing volumes and the challenge of handling small samples. In contrast to bulk materials, there is neither a standard procedure nor a commonly accepted methodology to follow. However, increasing efforts have been made, and several different test methods are proposed and used. The methodologies used to measure the fracture toughness of thin films are bending, buckling, scratching, indentation, and tensile tests.[8] To study multiple cracking phenomena of brittle films on compliant substrates, in situ fragmentation tests have been conducted.[9–12] This method, in which the progressive development of crack density in the coating is analyzed as a function of substrate elongation, has proven to be efficient for (i) the determination of the strength distribution in the film and the type of strain transfer (linear or nonlinear) between film and substrate[9,13] and (ii) the calculation and modeling of adhesive and cohesive fracture toughness.[10,14–17] More direct measurements of fracture toughness of thin films on compliant substrates are possible by bulge testing of circular membranes[18] and a special buckling test.[19] Here, the fracture toughness is directly obtained from the measured fracture stress and strain, respectively.

In this study, we investigate the thickness dependence for multiple cracking of Cu films (34–506 nm thick) on polyimide substrates with Ta interlayers (3.5–19 nm thick). By combining the results of in situ tensile tests in a scanning electron microscope (SEM) and a novel synchrotron-based tensile testing technique[20–22] on identical samples, various parameters of the fracture behavior are obtained. By the synchrotron technique, the stress-strain evolution in the Cu film during cracking is monitored, whereas by SEM, the crack evolution can be visualized, and crack spacing and crack opening can be quantified. In addition, an energetic approach is proposed, by which the energy release rate for a given strain/crack density is estimated from the difference in measured volume energy (area under measured stress-strain

[a)]Present address: Universität Karlsruhe, Institut für Zuverlässigkeit von Bauteilen und Systemen, D-76131 Karlsruhe, Germany.
[b)]Address all correspondence to this author.
e-mail: ralph.spolenak@mat.ethz.ch
DOI: 10.1557/JMR.2009.0252

curve) and the volume energy of a fully plastic film (area under imaginary stress plateau). By stepwise integration, the fracture toughness evolution during multiple cracking can be determined. The data provide further insight in the fracture mechanics of thin films on compliant substrates and the role of decreasing ductility in very thin films.

The results are discussed in the light of thin film fracture mechanics models for stiff films on compliant substrates dealing with statistical aspects,[9,13] linear elastic fracture mechanics,[23,24] substrate deformation,[25,26] film/substrate interaction,[27,28] and strain localization and debonding.[11,29–31] It seems that the fracture mode in the ductile Cu layer is related to local necking in the regions of initial cracks in the brittle Ta layer. The scaling behavior of fracture toughness and the crack shape imply, however, an increasing inherent brittleness of Cu films with decreasing thickness.

II. EXPERIMENTAL

A. Sample preparation

Two sets of Ta/Cu film systems with varying Cu and Ta film thickness and a set of 10-nm-thick Ta films were prepared (Fig. 1). The first Ta/Cu set consisted of 30- to 500-nm-thick Cu films deposited on an about 10-nm-thick Ta interlayer and the second of 80-nm-thick Cu films deposited on Ta interlayers with 4–20 nm thickness. As substrate, 125-μm-thick dogbone-shaped polyimide foils (Kapton HN, DuPont, Wilmington, DE) with a gauge section of 6 mm × 20 mm were used. Before film deposition, the substrate surface was sputter cleaned for 1 min using an Ar^+ plasma (105 V, 0.8 A). Cu and Ta films were deposited onto the electrically grounded polyimide substrates using a direct-current (DC) magnetron sputter deposition system with a base pressure of 1×10^{-8} mbar, a DC power of 200 W (Cu) and 100 W (Ta), and an Ar pressure of 4.2×10^{-3} mbar. The corresponding deposition rates were 45 (Cu) and 12 nm/min (Ta), respectively. After deposition, all samples were annealed in the deposition chamber at 350 °C for 0.5 h. The microstructure of the films was checked by electron backscatter diffraction (EBSD) and plan-view transmission electron microscopy (TEM).[22] All films showed a homogeneous microstructure with equiaxed columnar grains and with a median grain size that is slightly larger than the film thickness.

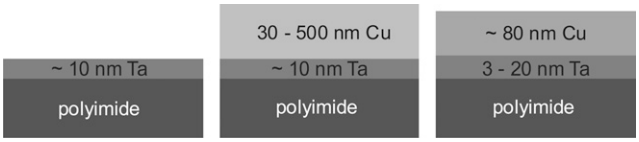

FIG. 1. Schematic drawing of the Ta and Ta-Cu film systems investigated. The Ta and Cu film thicknesses were varied.

The film thickness of the individual metallic layers was determined by Rutherford backscattering spectrometry (RBS). All RBS measurements were conducted using 2 MeV He^+ ions (6.5-MV Pelletron accelerator at the Max Planck Institute for Metals Research, Stuttgart, Germany). The film thickness of the Cu and the Ta films could be obtained by fitting the RBS spectra of the Si detector with the X-Rump simulation software (Computer Graphics Service Ltd., www.genplot.com) taking into account the scattering geometry, ion species, and energy.

The following sample denotation will be used to classify the different samples investigated in this study: Ta-*x*-Cu-*y*. The variables *x* and *y* represent the corresponding Ta and Cu film thickness measured by RBS in nanometers. For all samples, the Ta layer lies in between the polyimide substrate and the Cu film.

B. Mechanical testing

The experimental procedure and data analysis, as well as the unique features concerning the synchrotron-based tensile testing technique, are described in detail in Ref. 20. The necessary modifications for the adaptation of this technique to Cu films are listed elsewhere.[21,22] All tensile tests were performed at the MPI-MF-beamline located at the synchrotron radiation source ANKA (Angströmquelle Karlsruhe). For the tensile tests of this study, the maximum total strain of the samples was increased up to 7.5%. During the tensile test, the crosshead displacement of the tensile tester (Kammrath & Weiss, Dortmund, Germany) was varied in steps between 30 and 100 μm. The total strain of the sample was measured by a laser-extensometer (Fiedler Optoelektronik, Lützen, Germany). It was not possible to determine the stress in the Ta layers because the diffracted intensity was below the detection limit.

In addition to the tensile tests at the synchrotron, in situ tensile tests in a scanning electron microscope were conducted on the same sets of samples. Here the tensile tester was mounted on the sample stage of an SEM (Leo 1530VP, Carl Zeiss, Oberkochen, Germany). The samples were loaded again in a stepwise manner, and SEM images were taken for every step. The total strain on the samples was obtained from the crosshead displacements by calibration with the laser extensometer measurements at the synchrotron. For the SEM tests, the maximum total strain was 20%. To determine the crack spacing, two different methods were applied. At small strains, cracks did not span the complete width of the SEM images, so the mean crack spacing was defined as total crack length (along the film plane) per image area. At large strains, at least 30 cracks were counted on the micrographs along multiple straight lines drawn perpendicular to the cracks, and this number was divided by the total line length. In a similar way, the crack opening was determined for different total strains from the length of these lines within the cracks.

III. RESULTS

A. Stress-strain curves

In the following, results from synchrotron tensile tests on Ta-Cu film systems on polyimide with different Cu and Ta film thickness are presented. Figures 2(a) and 2(b) show the stress evolution in the longitudinal and transverse directions in 67- and 506-nm-thick Cu films, respectively.

In general, the absolute stress values were higher for the thinner film. After an initial linear elastic regime, the films deformed plastically up to total strains of about 2.5%. For higher strains, the longitudinal and transverse stresses began to decrease. This decrease was much more pronounced for the 67-nm film. For the 506-nm film, it is almost not visible. On unloading, a compressive stress state developed in both Cu films because they had been plastically deformed, whereas the polyimide substrates deformed elastically during the whole tensile test. The tensile (loading) and compressive (unloading) stresses in transverse direction resulted from the mismatch in Poisson's ratio of Cu and polyimide.[22] Only the longitudinal stresses of each sample are plotted in Figs. 2(c) and 2(d) to facilitate the comparison between the films. The length of the elastic regime depends on the initial residual stress of the film, which can vary because of processing and can already be close to the yield strength of the film. The stress maximum and the amount of stress release increased with decreasing Cu film thickness. A decreasing Ta thickness resulted in an increase of the stress maximum, whereas the stress release were similar.

B. Fractography

Figure 3 shows a representative set of SEM micrographs of one Ta-9nm film and Ta-9nm-Cu-*y* films with different Cu film thickness. Except for Fig. 3(d), all micrographs were taken at a similar total strain between 6.25 and 6.82% under stress. The crack evolution in all films was very similar. At low strains, short primary cracks nucleated in the film and grew perpendicularly to the loading direction. The length of the cracks was much smaller than the width of the sample. For higher strains, the existing cracks grew further, and new cracks nucleated between the existing cracks. The number of cracks and the crack shape depended on film material and film thickness. The Ta-9nm film showed the smallest crack spacing, and the cracks were straight. A similar crack shape was observed for the Ta-9nm-Cu-34nm sample but with larger crack spacing. With increasing Cu film thickness, the crack spacing further increased, and the cracks became shorter and more irregular. For the Ta-9nm-Cu-506nm sample, almost no cracks were visible at the surface for a total strain of 6.82%. Figure 3(d) shows a Ta-9nm-Cu-67nm sample strained up to 23.02%. For strains >15%, secondary cracks formed

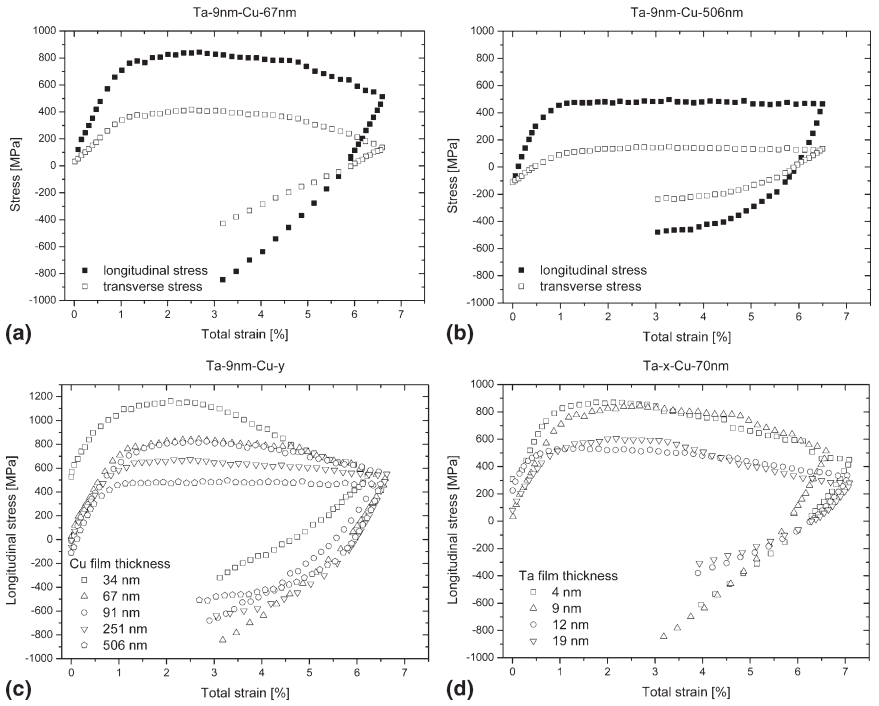

FIG. 2. Stress-strain curves for different Ta-Cu film systems measured by the synchrotron-based tensile testing technique. The longitudinal (filled symbols) and transverse stresses (open symbols) are shown for (a) a 67- and (b) a 506-nm-thick Cu film. Variations in (c) Cu and (d) Ta film thickness influence the maximum stress and the amount of stress release. For a clearer overview, only the longitudinal stresses are compared. (d) The Cu film thickness for the Ta-*x*-Cu-70nm samples varied between 67 and 71 nm.

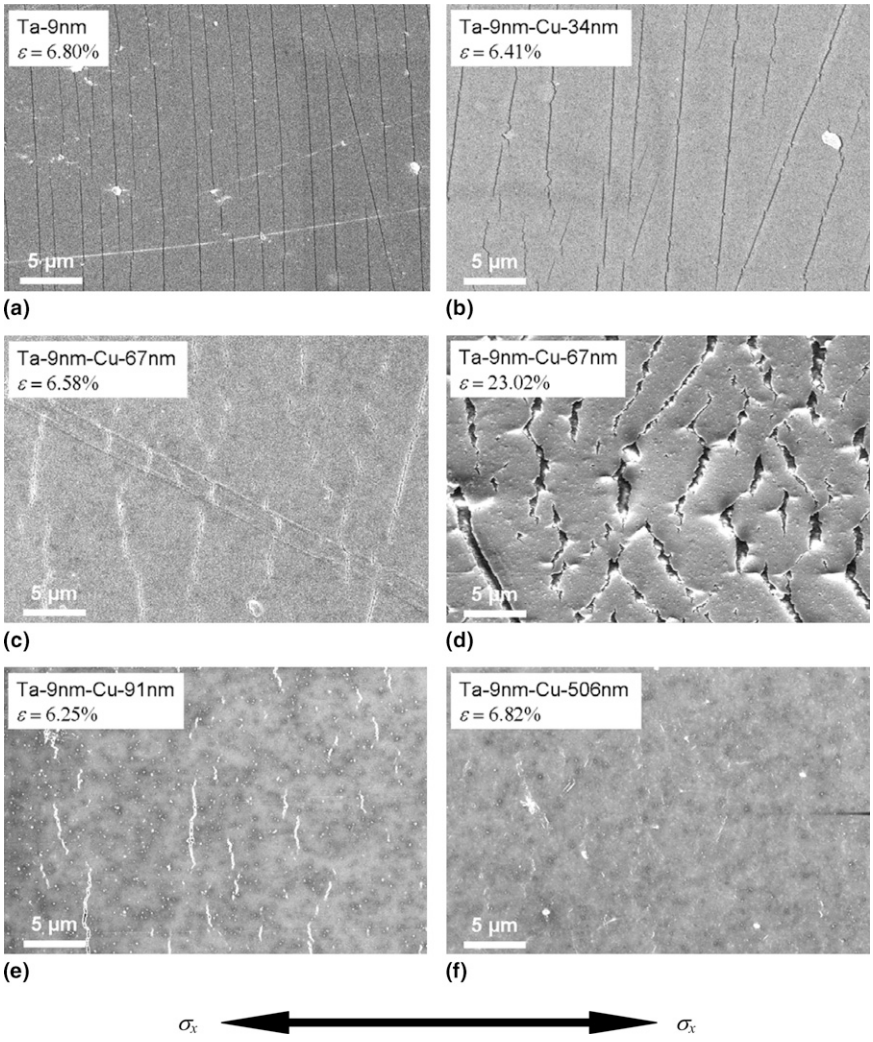

FIG. 3. SEM micrographs of a Ta-9nm and different Ta-9nm-Cu samples. (a)–(c), (e), and (f) were taken at a similar total strain of about 6.5%. Primary cracks nucleate and grow perpendicularly to the loading direction (black arrow at the bottom). Crack spacing and shape depends on film material and film thickness. (d) Ta-9nm-Cu-67nm sample strained up to 23.02% total strain. Secondary cracks form at the edge of primary cracks.

parallel to the loading direction starting at the crack front of a primary crack.

From the complete set of SEM pictures, the mean crack spacing L and crack opening displacement δ was determined. In Figs. 4(a)–4(c), the mean crack spacing is plotted as a function of total strain for the Ta-9nm sample and the different Ta-Cu film systems. The overall shape was again similar. In the beginning, the crack spacing decreased rapidly with strain. Subsequently, the slope changed gradually leading to a smaller slope at larger strains. However, the absolute crack spacings are different. An increase in Cu film thickness led to an increase in crack spacing and to higher onset strains for cracking. Thus, for the thicker films, the second regime with the smaller slope was not reached for strains up to 20%. On the other hand, an increase in Ta film thickness resulted in a decrease of the initial crack spacing, whereas the final crack spacing was nearly independent of Ta film thickness. In addition, lower onset strains were found for thicker Ta interlayers. For comparison, the initial slope was higher and the crack spacing was much smaller for the Ta-9nm film.

Before and after the change in slope, power-law functions in the form

$$L = c\varepsilon^{-\kappa} \quad , \tag{1}$$

where L is the crack spacing, ε the total strain, and c a constant number, were fitted to the experimental data.[9,13] The intersection of the two power-law functions was used to define the crossover values for total strain and crack spacing, ε_c and L_c, respectively [Fig. 4(a)]. Table I summarizes the power-law exponents κ_1 (before crossover) and κ_2 (after crossover) and the resulting values of ε_c and L_c. In Fig. 4(d), the crack opening is plotted against the total strain for different Ta-9nm-Cu film systems. The crack opening increased linearly with

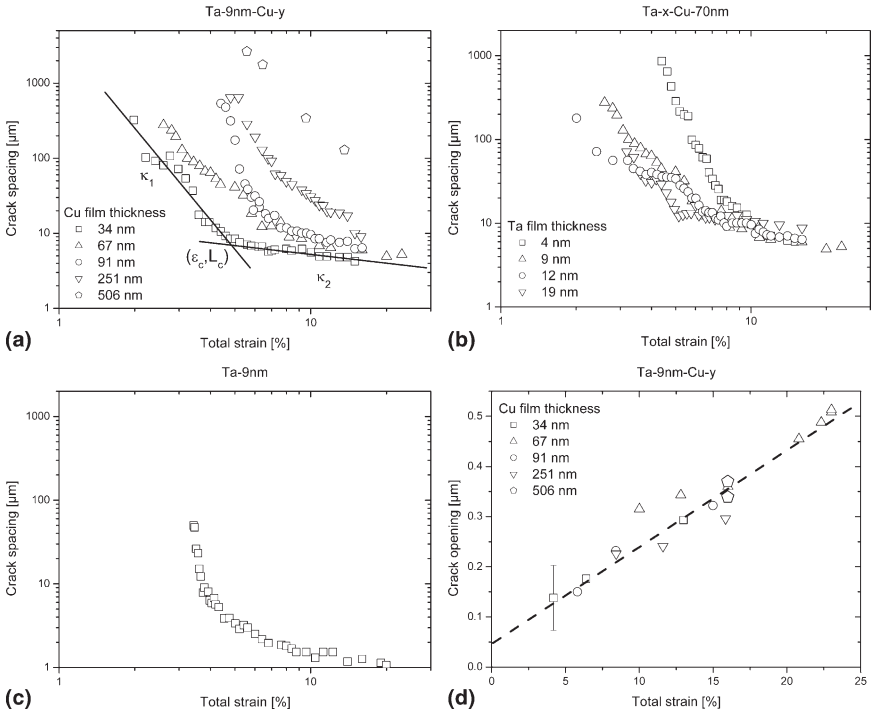

FIG. 4. Mean crack spacing versus total strain for (a, b) Ta-Cu-film systems and (c) a Ta-9nm sample. The Cu film thickness for the Ta-*x*-Cu-70nm samples in (b) varied between 67 and 71 nm. The overall shape of the curves is similar, whereas absolute values depend on Cu and Ta film thickness. (d) Crack opening versus total strain for Ta-Cu film systems with varying Cu film thickness. The crack opening increases with strain and is independent of Cu film thickness.

TABLE I. Fragmentation parameters for the different Ta-Cu film systems and the Ta-9nm film.

Sample	κ_1	κ_2	ε_c	L_c (μm)	m
Ta-9nm-Cu-34nm	4.1 ± 0.5	0.42 ± 0.07	0.049	6.9	0.90 ± 0.2
Ta-9nm-Cu-67nm	4.4 ± 0.5	0.44 ± 0.08	0.055	8.9	0.96 ± 0.2
Ta-9nm-Cu-91nm	8.9 ± 0.7	(0.66)	(0.067)	(11.5)	
Ta-9nm-Cu-251nm	6.1 ± 0.4	(0.71)	(0.086)	(25.0)	
Ta-9nm-Cu-506nm	4.2 ± 0.3				
Ta-4nm-Cu-71nm	8.8 ± 0.5	0.47 ± 0.09	0.075	8.5	0.99 ± 0.3
Ta-12nm-Cu-70nm	2.3 ± 0.5	0.39 ± 0.08	0.065	8.9	0.96 ± 0.3
Ta-19nm-Cu-71nm	3.4 ± 0.3	0.42 ± 0.08	0.052	11.1	0.91 ± 0.2
Ta-9nm	19.6 ± 1.6	0.47 ± 0.12	0.040	2.3	0.94 ± 0.3

Listed are the two scaling exponents κ_1 and κ_2, the crossover values of the total strain ε_c, and crack spacing L_c, as well as the nonlinearity parameter of the strain transfer m (Sec. IV. A). The values in parentheses are uncertain because the change in slope was not accomplished for these samples. For the Ta-9nm-Cu-506nm sample, no change in slope was observed within the investigated strain range.

strain for all film systems and does not depend on film thickness. A collection of the values for the initial crack spacing L_0 at the onset of cracking, the intermediate crack spacing L_i at a total strain of about 6.5% (slightly below maximum total strain of synchrotron experiments), the final crack spacing L_f for a total strain of 16% at the end of the tensile tests in the SEM, and the initial crack opening displacement δ_0 is given in Table II.

IV. DISCUSSION

Unlike methods to determine fracture toughness for bulk specimens, where the largest defect determines the behavior, the substrate suppresses strain localization in the thin film systems studied. Thus, not only the largest defects are probed, but the entire distribution of defect sizes can be studied and analyzed. In the following, the crack evolution as a function of the applied strain will be analyzed for different film thicknesses. In addition, this study focuses on the fracture behavior of a ductile material, and thus, plasticity needs to be included in the fracture analysis. In contrast to classical fracture mechanics for bulk materials, the following points need to be observed:

(i) The Cu films already deform plastically before fracture occurs, which is violating the assumption made for classical elastic plastic fracture mechanics, namely

TABLE II. Initial crack spacing L_0 (onset of cracking), intermediate crack spacing L_i ($\varepsilon \approx 6.5\%$), final crack spacing L_f ($\varepsilon \approx 20\%$), and initial crack opening displacement δ_0 for different Ta-Cu film systems.

Sample	L_0 (μm)	L_i (μm)	L_f (μm)	δ_0 (μm)
Ta-9nm-Cu-34nm	102.7	6.8	4.7	293
Ta-9nm-Cu-67nm	285.6	15.0	6.4	295
Ta-9nm-Cu-91nm	534.3	26.1	8.1	292
Ta-9nm-Cu-251nm	652.1	193.5	18.7	278
Ta-9nm-Cu-506nm	2696.5	2185.8	128.1	302
Ta-4nm-Cu-71nm	865.0	85.5	6.1	245
Ta-12nm-Cu-70nm	182.8	20.1	6.5	251
Ta-19nm-Cu-71nm	72.5	12.4	9.1	293

The values are obtained by analyzing the SEM micrographs by eye, and the error is assumed to be 10% for the crack spacing and 30% for the crack opening displacement.

the plastic zone being small in comparison to the specimen dimensions.

(ii) The analysis of our data by a linear elastic approach should always result in toughnesses that are lower than the ones calculated by an analysis that includes plasticity, and consequently, linear elastic analysis (even if not appropriate) should be included to serve as a baseline to validate the plastic fracture mechanics analysis concept.

The discussion is divided into three parts: crack spacing analysis, linear elastic fracture toughness analysis, and fracture toughness analysis including plasticity. For the latter case, we introduce a concept based on the data collected as classical approaches are not viable for the reasons given above.

A. Crack spacing analysis

The evolution of the mean crack spacing L with total strain ε for the Ta-Cu-film systems and the Ta-9nm sample can be approximated by two power laws both at the onset and the later stage of cracking [Fig. 4(a)]. Handge[9] and Handge et al.[13] have shown that, for thin brittle films on ductile substrates, the power-law exponents κ_1 and κ_2 are related to the strength distribution in the film and are not independent. The correlation between κ_1 and κ_2 is given by the fact that the stress in the film is locally reduced around a crack. In the initial stage of cracking, the average strain in the film equals the total strain of the film/substrate composite. This leads to the formation of cracks at locations given by the statistical distribution of flaws in the film. With ongoing sequential cracking and decreasing crack spacing, the stress in the film becomes more and more nonuniform, with maximum values in the midsection between two preexisting cracks. New cracks form predominantly in the highly stressed regions, and thus, the location of the cracks is no longer random. According to the analysis by Handge[9] and Handge et al.,[13] κ_1 is equal to the Weibull exponent α of the strength distribution of the film, and κ_2 depends on both α and m, where m is the nonlinearity parameter of the strain transfer between film and substrate, according to:

$$\kappa_2 = \frac{m\alpha}{(m+1)\alpha+1} = \frac{m\kappa_1}{(m+1)\kappa_1+1} \quad . \qquad (2)$$

For a linear strain transfer $m = 1$, and κ_1 as well as κ_2 depend only on α, whereas $0 < m < 1$ holds for a substrate material that deforms plastically or viscoelastically. By combining the results for κ_1 and κ_2, one can determine experimentally the parameters for the Weibull distribution of defects and the nature of strain transfer between film and substrate.

Solving Eq. (2) for m and using the experimental values for κ_1 and κ_2, m is found to be between 0.9 and 0.99 for our Ta and Ta-Cu film systems (Table I). This indicates a predominantly linear elastic strain transfer between the Ta and Cu films and the polyimide substrate. This is also corroborated by the fact that the crack opening displacement increases linearly with external strain [Fig. 4(d)]. For the thicker Ta-9nm-Cu films, the transition to the second power law could not be observed accurately, and m consequently could not be analyzed.

The experimental values for κ_1 of the Ta-9nm-Cu film systems show no clear trend as a function of Cu film thickness. This may be because of sample preparation. In principle, modern sputtering techniques produce films with low flaw densities, and most defects are located at the film/substrate interface. For our film systems, the situation is even aggravated because the Ta interlayers, which are the most brittle part, are neighboring regions of high defect density. Therefore, we assume that crack nucleation occurs at the Ta/polyimide interface and cracks propagate instantly into the Ta layer. In addition, the dogbone-shaped polyimide substrates have been prepared mechanically, which induces some scratches on the substrate surface. Scratches are favorable crack nucleation sites and may broaden the strength and defect distribution of the final film. The occurrence of these additional scratches is not systematic and may explain the inconsistent variation of κ_1. For the Ta-*x*-Cu-71nm samples, the situation is different. The initial flaw size at the interface is expected to be comparable to the scenario above. However, as the initial flaws cause cracks in the Ta interlayer, the Ta film thickness, which is varied systematically, determines the critical defect size for crack propagation into the copper layer. Thus, it is reasonable to assume that the initial crack size and size distribution increases with increasing Ta film thickness, which results in lower values for κ_1. Compared with the Ta-Cu film systems, the Ta-9nm sample shows a much higher value for κ_1 (two to six times higher). Here, the cracks do not need to propagate into a ductile copper layer and therefore already very small defects lead to instantaneous fracture of the brittle Ta film.

The crossover values for total strain ε_c and crack spacing L_c show clearer trends (Table I). L_c scales directly with the total thickness of the samples (Ta plus Cu film thickness). This can be attributed to the size of the stress relaxation zone around the cracks, which increases with increasing film thickness.[13,24] It leads to larger crack spacing because the distance until the stress reaches the fracture stress becomes larger. The crossover strain ε_c decreases with increasing Ta film thickness, which can be explained by the increasing defect size, but increases with increasing Cu film thickness. The latter observation cannot be explained by a Weibull strength distribution because the probability of a critical defect would increase with increasing film thickness leading to decreasing fracture strains.[10,15]

B. Linear elastic fracture mechanics as a baseline

Crack propagation in a film bonded to a substrate is a three-dimensional process. Nevertheless, for steady state, channel cracking of brittle films (no plastic deformation) on substrates can be described analytically by two-dimensional models.[23,24] Xia and Hutchinson[24] have shown that the longitudinal stress change $\Delta\sigma_x$ (perpendicular to the crack and parallel to the loading axis x) caused by stress relaxation at the crack front is

$$\Delta\sigma_x = \sigma_0 \exp(-|x|/l) \quad , \tag{3}$$

where σ_0 is the mean stress in the Cu film before cracking (maximum stress in the stress-strain curves) and l is a reference length characterizing the exponential decay of the stress:

$$l = \frac{\pi}{2} g(\alpha, \beta) h \quad . \tag{4}$$

Here h is the film thickness. The quantity $g(\alpha, \beta)$ represents the dimensionless integral of the crack opening displacement as defined by Beuth,[23] with α and β being the two Dundur's parameters[32] characterizing the elastic mismatch between film and substrate. For a compliant film on a stiff substrate, $g(\alpha, \beta)$ is about 0.8–1.2, whereas it reaches values of 20 and more when the film is stiff compared with the substrate.[23] For our case of Ta and Cu films on polyimide, $g(\alpha, \beta)$ is estimated to be 15 (α = 0.97). Therefore, l is about 24 times the film thickness (Table III). Subsequently, the average longitudinal stress σ_x in the film can be calculated[21]:

$$\sigma_x = \sigma_0 - \frac{\int_0^{L/2} \Delta\sigma_x dx}{\int_0^{L/2} dx} = \sigma_0 \left(1 + \frac{\exp(-L/2l) - 1}{L/2l}\right) \quad . \tag{5}$$

In Fig. 5, σ_x is plotted against the total strain and compared with the longitudinal stress measured during the synchrotron experiments for the Ta-9nm-Cu-67nm and Ta-9nm-Cu-251nm sample. The necessary values for σ_0 and l can be found in Table III. The corresponding crack spacing is taken from Fig. 4(a). This method may still be applied for a plastically deforming material because the unloading of the material is in first approximation a purely elastic process.

TABLE III. Mean stress σ_0 before cracking as determined from Figs. 2(c) and 2(d) and results for the reference length l, the energy release rate G_{Beuth}, and fracture toughness $K_{C,Beuth}$.

Sample	σ_0 (MPa)	l (μm)	G_{Beuth} (J/m^2)	$K_{C,Beuth}$ (MPam$^{1/2}$)
Ta-9nm-Cu-34nm	1151	1.013	6.0	1.03
Ta-9nm-Cu-67nm	842	1.791	6.4	1.06
Ta-9nm-Cu-91nm	822	2.356	8.3	1.20
Ta-9nm-Cu-251nm	666	6.126	14.9	1.62
Ta-9nm-Cu-506nm	487	12.134	16.1	1.68
Ta-4nm-Cu-71nm	872	1.767	7.2	1.13
Ta-12nm-Cu-70nm	539	1.956	2.7	0.69
Ta-19nm-Cu-71nm	603	2.121	3.5	0.78

The values were calculated according to Eqs. (4), (6), and (7).

It is evident that the calculated stress values fit well to the experimental values for the thinner sample, at least for the initial stage of cracking. This indicates that in the beginning the thinner sample behaves like a brittle material. For >5% total strain, the measured stress values begin to deviate and become lower than the calculated ones. This strain level correlates with the transition from the first power-law regime for crack spacing to the second (the crossover strain ε_c for the Ta-9nm-Cu-67nm sample is 0.055; Table I). Here, the crack spacing becomes comparable to $2l$ and the analysis of a single crack may no longer be valid. For the thicker samples, the calculated values deviate from the experimental ones already in the first power-law regime (ε_c for the Ta-9nm-Cu-251nm sample is 0.086).

Beuth[23] has shown that the energy release rate G_{Beuth} associated with the steady-state crack propagation in a brittle film on a substrate of infinite thickness is given by:

$$G_{Beuth} = \frac{\pi}{2} \frac{(1 - \nu_f^2)\sigma_0^2 h}{E_f} g(\alpha, \beta) \quad . \tag{6}$$

Subsequently, the fracture toughness $K_{C,Beuth}$ for plane strain can be obtained by[33]:

$$K_{C,Beuth} = \sqrt{\frac{E_f G_{Beuth}}{(1 - \nu_f^2)}} \quad , \tag{7}$$

where E_f and ν_f are the Young's modulus and Poisson's ratio of the film material, respectively. Because of the strong (111) fiber texture of the Cu films, the Young's modulus $E_{Cu[110]}$ = 130 GPa for the [110] direction and

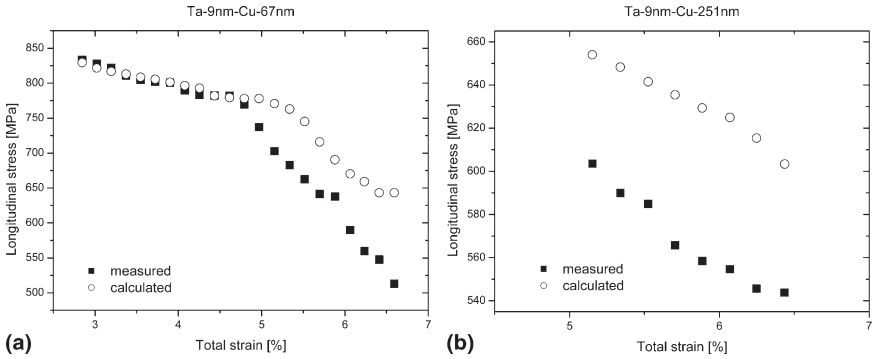

FIG. 5. Longitudinal stress measured by the synchrotron technique and calculated according to Eq. (5) versus total strain for (a) the Ta-9nm-Cu-67nm and (b) the Ta-9nm-Cu-251nm sample. Good agreement between measured and calculated values is obtained in the initial stage of cracking for the thinner sample.

the Poisson's ratio $\nu_{Cu(111),\ [110]} = 0.51$ for the (111) plane in the [110] direction are used.[22] Based on our experimental results, $K_{C,\ Beuth}$ varies between 0.69 and 1.68 MPam$^{1/2}$ (Table III). Despite the expected trends of increasing fracture toughness for increasing Cu film thickness or decreasing Ta film thickness, the absolute values are extremely low for a face centered cubic (fcc) metallic material. This is a similar argument to the stress calculations above. Both results indicate that stress in the Ta-Cu-film systems is not only released by brittle fracture, but additional stress relaxation processes must take place. Possible mechanisms may be substrate deformation,[25–28] strain localization in the film,[11,29–31] or plasticity of the metallic films.[34]

The energy release rate for channel cracking in a film bonded to a substrate can be significantly affected by the substrate properties. The two-dimensional elastic plane strain analysis presented above has been extended to substrates of finite thickness[26] and to elastic-plastic substrates.[25] The corresponding results show that $g(\alpha, \beta)$ can increase by a factor of 2–3 for thin substrates ($h_s/h_f < 100$, h_s: substrate thickness) or substrates with low yield strength ($\sigma/\sigma_{y,s} > 2$ with macroscopic stress σ and substrate yield strength $\sigma_{y,s}$). Neither is the case for our Ta-Cu films on polyimide ($h_{polyimide}/h_{Ta\text{-}Cu}$ = 240–3000, $\sigma/\sigma_{y,polyimide}$ = 0.6–1). Begley and colleagues[27,28] have proposed a different approach considering the interaction between the film, the substrate of finite thickness, and stiffness, as well as the crack spacing and opening. According to their model, the effective modulus of the cracked film/substrate composite is lower than that of the intact sample, and the steady-state energy release rate can be calculated by the stress in the intact portion of the metallic film and the crack opening displacement. However, this analysis is also not applicable to our data because the polyimide substrate is too stiff compared with the boundary conditions of their model.

Xiang et al.[11] and Li and colleagues[29–31] have shown that, if a metallic film is fully bonded to a polyimide substrate, the substrate suppresses large local elongations in the film. Thus, the film may deform uniformly up to high total strains. However, if the film debonds locally from the substrate, it becomes freestanding and ruptures at a smaller strain than the fully bonded film. To reduce the rupture strain to a few percent as observed in our experiments (2–4%), the debond length would have to be about 100 times the film thickness.[30] Such debond lengths are unreasonable for our samples because the ratio between the crack spacing and film thickness L_f/h_f is only 75–200, which means that the complete film would have to delaminate. Nevertheless, the initial cracks in the Ta interlayer represent sites of local debonding, and it seems that they are crucial for the subsequent cracking of the Cu films because experiments on similar Cu films without Ta interlayer showed homogeneous deformation up to high total strains and no fracture.[22] SEM after etching of the Cu film of a fractured Ta-Cu sample showed an identical crack pattern in the remaining Ta film compared with the Cu film, without indicating considerable additional debonding.

C. Fracture toughness analysis including plasticity

In principle, it is possible to determine the fracture toughness from the multiple cracking data by sophisticated finite element modeling.[16,17] However, for such an analysis, the fracture mechanisms must be known and implemented in the model. In the following, we propose a more direct data analysis approach based on the combination of the results for in situ tensile tests in the SEM and the synchrotron. Because of the substrate constraint, the stress in the film relaxes only locally around the crack.[23,24] In between the cracks, the strain transfer from the substrate to the film is still intact and stress does not relax. Assuming that the adhesion between the metallic films and the polyimide substrate stays intact and no debonding takes place, any release in volume energy of the film can be attributed to the crack formation. The energy release by cracking can be estimated from the

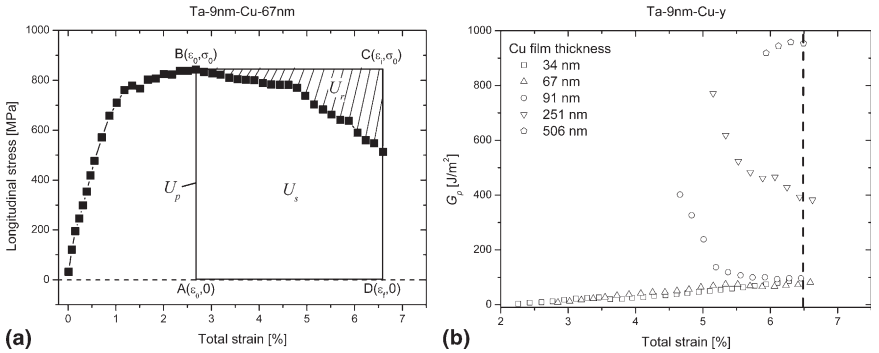

FIG. 6. (a) Schematic illustration of the data analysis. A constant stress plateau for a film without cracks is assumed. (b) Energy release rate G_p versus total strain for different Ta-9nm-Cu film systems. For thinner films, an increase in energy release rate is found, whereas for thicker films, G_p decreases with strain. At 6.5% total strain, G_p becomes almost constant for all film systems.

stress-strain curves measured by the synchrotron technique [Fig. 6(a)]. The volume energy U_s stored in the Cu film is given by the area under the measured stress-strain curve. Experiments on Cu films without cracks have shown that, after yielding and strain hardening, a stress plateau is reached for strains $>1.5\%$[22] and remains up to total strains of about 7%.

Because the stress decrease in this study always starts at least at 2.5% total strain, we assume that the plateau stress has already been reached, and without cracking, the stress in the Cu film would remain constant. Even for the Ta-9nm-Cu-34nm sample, which showed the highest flow stress, the slope before the stress decrease is almost zero [Fig. 2(c)]. Doing so, we can estimate the volume energy U_p for a film without cracks and calculate the volume energy U_r released by the cracks:

$$U_r = U_p - U_s = \sigma_0(\varepsilon_i - \varepsilon_0) - \int_{\varepsilon_0}^{\varepsilon_i} \sigma(\varepsilon) d\varepsilon \quad , \qquad (8)$$

where σ_0 is the longitudinal stress before the stress decrease, ε_0 is the corresponding strain, and ε_i is the upper cut-off strain. To obtain the energy release rate G_p for cracking (energy release per unit crack area), U_r was related to the created crack area A_c:

$$G_p = \frac{U_r V}{A_c} = \frac{U_r h w L_i}{h w} = U_r L_i \quad , \qquad (9)$$

where V is the volume around a crack (estimated as distance of $L/2$ on both sides of the crack), h the film thickness, w the width of the sample, and L_i the mean crack spacing at ε_i. The crack spacing is obtained from the in situ SEM experiments [Figs. 4(a) and 4(b)].

By integration of the stress-strain curves (using Origin 7 SR2 v7.0383; OriginLab, Northampton, MA) and evaluating the crack spacing for every strain step, the energy release rate G_p in the Cu film was obtained as a function of total strain. In Fig. 6(b), the corresponding results for the Ta-9nm-Cu samples are shown. It is evident that the energy release rate increases with Cu film thickness. The thinnest samples also show an increasing energy release rate with total strain. In contrast, the energy release rate decreased with increasing total strain for the samples with 91- and 251-nm Cu film thickness. For the thickest sample with 506-nm Cu film thickness, a slight increase is observed. This, again, reflects the transition from a completely brittle to a more ductile behavior of the Cu films. For the thinnest and brittle samples, the energy release rate increases because fracture starts at the largest defects, which are subsequently eliminated, and the defect size distribution is shifted to smaller defects. For the thicker and more ductile samples, plasticity around the defects may lead to local strain hardening and an increasing brittleness, which is reflected in the decreasing energy release rate. The 506-nm-thick Cu film may deform completely homogenously by plastic flow, resulting in an almost constant energy release rate.

For a total strain of about 6.5%, the energy release rate became almost constant for all samples. The energy release rate $G_{p,6.5}$ at 6.5% total strain is thus taken to calculate the fracture toughness $K_{C,p,6.5}$ of the Cu films by Eq. (7). The integration limits ε_0 and ε_i, the evaluated values for the volume energies U_s and U_r, and the results for the energy release rate and fracture toughness are listed in Table IV. The values for the corresponding crack spacing L_i and σ_0 can be found in Tables II and III, respectively. In Fig. 7, $K_{C,p,6.5}$ is plotted as function of film thickness and compared with the results of the linear elastic fracture mechanics analysis. It increases roughly linearly with increasing Cu film thickness, whereas it decreases with increasing Ta film thickness. The absolute values are considerably higher than those for $K_{C,\text{Beuth}}$ and vary from 2.73 to 12.68 MPam$^{1/2}$. This is also in contrast to existing studies on brittle thin films on substrates, where no distinct change in fracture toughness[35,36] or decreasing fracture toughness with increasing film thickness[15] has been found. In addition, the absolute values are considerably higher compared with results for 150-nm-thick Al films on polyimide (K_{IC} = 2.04 MPam$^{1/2}$)[18] and 0.8-μm-thick Cu-Sn intermetallic

TABLE IV. Input data and results for evaluation of energy release rate $G_{p,6.5}$ and fracture toughness $K_{C,p,6.5}$.

Sample	ε_0	ε_i	U_s (MJ/m^3)	U_r (MJ/m^3)	$G_{p,6.5}$ (J/m^2)	$K_{C,p,6.5}$ (MPam$^{1/2}$)
Ta-9nm-Cu-34nm	0.026	0.063	3138.4	10.9	74 ± 15	3.61 ± 0.34
Ta-9nm-Cu-67nm	0.027	0.066	2851.0	4.4	67 ± 12	3.42 ± 0.29
Ta-9nm-Cu-91nm	0.028	0.065	2586.4	3.8	100 ± 19	4.19 ± 0.38
Ta-9nm-Cu-251nm	0.027	0.066	2400.0	2.4	465 ± 107	9.04 ± 0.99
Ta-9nm-Cu-506nm	0.029	0.065	1692.3	0.4	915 ± 234	12.68 ± 1.53
Ta-4nm-Cu-71nm	0.027	0.061	2490.5	4.7	400 ± 59	8.39 ± 0.60
Ta-12nm-Cu-70nm	0.029	0.060	1449.0	2.1	42 ± 9	2.73 ± 0.29
Ta-19nm-Cu-71nm	0.029	0.061	1470.4	4.6	57 ± 11	3.18 ± 0.21

The parameters ε_0, ε_i, U_s, and U_r are described in the text and schematically shown in Fig. 6(a). $G_{p,6.5}$ and $K_{C,p,6.5}$ were calculated from these parameters according to Eqs. (9) and (7).

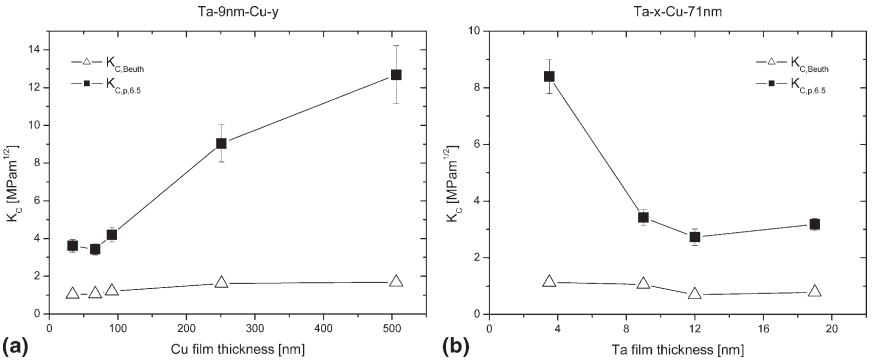

FIG. 7. Comparison of the experimentally observed fracture toughness $K_{C,p,6.5}$ and the fracture toughness $K_{C,Beuth}$ [see Eq. (7)] for samples with (a) varying Cu film thickness and (b) different Ta film thickness. The absolute values for $K_{C,p,6.5}$ are considerably higher and strongly depend on the Cu and Ta film thickness, respectively.

films on polyetherimide and polycarbonate substrates (K_{IC} = 2.63–2.83 MPam$^{1/2}$).[19] This clearly shows the need to include the stress relaxation by plastic deformation in the analysis of the fracture toughness.

Xiang et al.[11] have shown that Cu films well bonded to a polyimide substrate fracture by a mixture of local thinning and intergranular fracture. In contrast to strain localization, the substrate constraint is less effective in retarding intergranular fracture, because it needs little additional space to proceed. The same argument holds for cleavage fracture, also where no large local elongation occurs. Here, the presence of the substrate can only reduce the driving force for a long channel crack by limiting the crack opening in its wake. It is evident from Fig. 3 that in our Ta and Ta-Cu film systems, all fracture morphologies are present. The contribution of each type strongly depends on film thickness. Thin Ta and Ta-Cu samples show cleavage fracture with straight and tiny cracks [Figs. 3(a) and 3(b)], whereas Ta-Cu samples with intermediate thickness rupture by shorter and wider zig-zag cracks and local thinning [Figs. 3(c) and 3(e)]. The thickest Ta-Cu sample, however, shows only few and short zig-zag cracks, as well as some trenches, indicating an increasing tendency of necking [Fig. 3(f)]. In our opinion, the gradual change in fracture mechanism must be correlated to the increasing ductility of the Cu films with increasing film thickness, because the crack initiation (fracture of brittle Ta interlayer as discussed above) as well as the interface and the substrate properties are the same for all samples. Hsia et al.[34] also reported that, in very ductile fcc metals, cleavage fracture is possible because of dislocation confinement for submicron layers.

To quantify the contribution of plastic deformation during cracking of the Ta-Cu film systems, the volume averaged plastic strain ε_{pl} was calculated. This was done by dividing the initial difference between the stress according to the Beuth model [linear elastic, see Eq. (5)] and the experimental values obtained by the synchrotron technique (both for the first experimental values for the crack spacing, e.g., first data points in Fig. 5 for the Ta-9nm-Cu-67nm and Ta-9nm-Cu-251nm sample) by the Young's modulus of the film ($E_{Cu[110]}$ = 130 GPa). In Fig. 8, ε_{pl} is compared with the strain hardening $\sigma_{0.5}$–$\sigma_{0.1}$ and the flow stress $\sigma_{y,0.5}$ of identical samples with varying Cu film thickness.[22] For the two thinnest samples (h_f < 70 nm), ε_{pl} is zero because no difference between calculated and measured stress is found [see Fig. 5(a)], indicating that these samples show almost perfect brittle fracture. These samples also show a strong decrease in strain hardening and a saturation of flow stress. This is assumed to be correlated to a change in deformation mechanism from full to partial dislocations.[22]

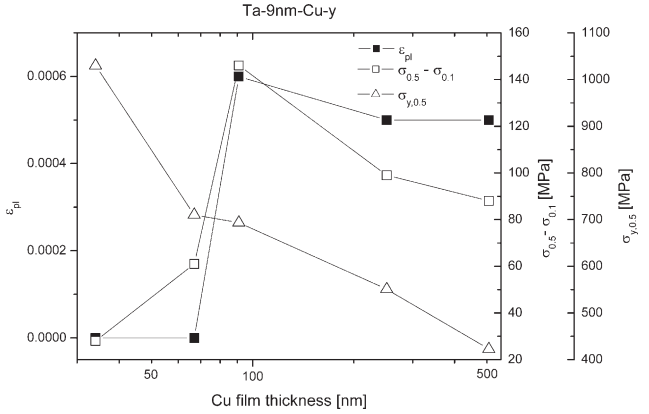

FIG. 8. Volume averaged plastic strain ε_{pl}, strain hardening $\sigma_{0.5}$–$\sigma_{0.1}$, and flow stress $\sigma_{y,0.5}$ for samples with varying Cu film thickness. Strain hardening and flow stress are replotted from a previous study.[22] Film systems exhibiting no volume averaged plastic strain also show little strain hardening and very high flow stress.

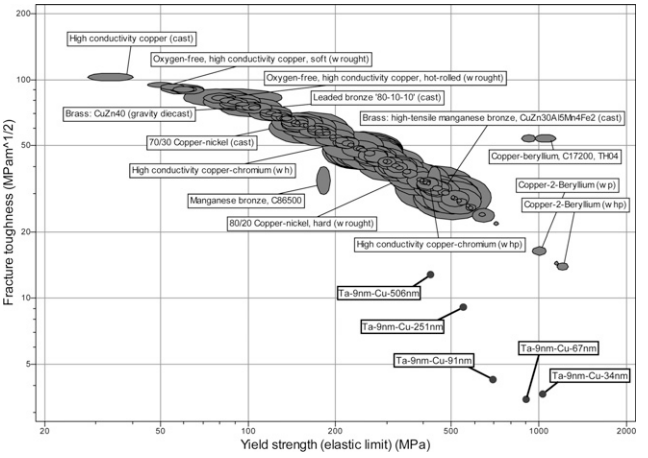

FIG. 9. Comparison of the measured fracture toughness for the different Ta-Cu film systems to literature data for pure Cu and Cu alloys with similar yield strength [CES Selector Version 4.6.1; Granta Design Ltd., Cambridge, UK].

The deformation by partial dislocations may not be efficient enough to sustain any crack initiation, leading to brittle fracture behavior. In contrast, for samples with a Cu film thickness >70 nm, ε_{pl} is about 0.04–0.07%, and the strain hardening (peak for $h_f \approx 90$ nm) and flow stress decrease with increasing Cu film thickness. Here, dislocation plasticity seems to relax some stress around the tip of the initial cracks in the Ta interlayer. This leads to the mixture of strain localization and brittle intergranular fracture.

Besides the increasing flow stress, the thin film geometry provides an additional effect on the fracture toughness. Compared with Cu alloys of similar flow stress, the fracture toughness of the Ta-Cu film systems is considerably lower (Fig. 9). On the other hand, the dependence on the flow stress is stronger for the thin film samples. This may be attributed to the geometrical constraint on the size of the plastic zone. Even if the films are already deforming plastically before fracture, it is instructive to evaluate this length scale. A rough estimation of the radius r_{pl} for the plane-strain plastic zone is given by[33]

$$r_{pl} \approx \frac{1}{6\pi}\frac{K_{IC}^2}{\sigma_y^2} \quad . \tag{10}$$

Inserting the experimental values for the different Ta-Cu film systems leads to an increasing radius for the plastic zone with increasing Cu film thickness from 0.5 to 36 μm, which corresponds to 10–40% of the final crack spacing or 10–70 times the film thickness. This clearly indicates that the contribution of plastic deformation increases with increasing film thickness and that the fracture toughness is limited by the thin film geometry. The fracture toughness of the Cu films thus depends on film thickness and is lower than that of a Cu-bulk material of the same strength.

In closing, three different aspects have to be considered to describe the fracture behavior of the Ta-Cu film systems under study. First, the Ta film thickness determines the initial defect size and thus the driving force to run cracks into the Cu films. This effect is found to be strongest for the thinnest Ta layer examined. For thicker ones, the variations in fracture toughness are marginal. Consequently, a comparison of systems with constant Ta thickness and varying Cu thickness seems reasonable. The absolute value of the Ta thickness is more important than the relative layer thickness. Ideally, fracture toughness of Cu should be independent of the dimension of a brittle layer. However, our analysis needs to be further improved to account for fracture in Ta by, for instance, also measuring the elastic strain in the Ta layer, which is an experimental challenge. Second, the Cu film thickness limits the size of the plastic zone and therefore leads to a reduced fracture toughness compared with the bulk material. Third, the dimensional constraint of the Cu film enhances its strength by dislocation–interface interaction and consequently reduces its ability to absorb strain energy by plastic deformation, resulting in a reduced ductility. Because the stress evolution could only be measured for the Cu films, the quantitative analysis of the fracture toughness of this study only reflects the answer of the Cu film to the crack nucleation within the brittle Ta film. For constant Ta film thickness, the apparent fracture toughness of the Cu film increases with increasing Cu film thickness because of the increasing ductility of the Cu film. If the Ta thickness is increased in a system of constant Cu thickness, the apparent fracture toughness decreases as more, and more strain energy originating from the Ta layer has to be absorbed by the constant plasticity of the Cu layer.

V. CONCLUSIONS

The cracking behavior of ultrathin Cu films on polyimide substrates with Ta interlayers was studied. The combination

of in situ tensile tests in a SEM and a synchrotron-based tensile testing technique has provided further insight in the fracture mechanics of thin films on compliant substrates.

(1) Sequential cracking of the films leads to a continuous and distinct decrease in the average stress of the film. Initially, the cracks form randomly according to the strength distribution in the film. Later on, the formation of new cracks depends on both the stress field determined by existing cracks and the closest flaws, which leads to a more regular crack spacing.

(2) By relating the release in volume energy by cracking, which could be estimated from the stress-strain curves of the Cu films, to the crack area determined from the in situ SEM tests, the fracture toughness of the Cu films can be obtained. The fracture toughness increases roughly linearly with Cu film thickness and decreases with increasing Ta film thickness.

(3) The measured values for the fracture toughness cannot be explained by existing models dealing with linear elastic fracture mechanics, substrate deformation, or strain localization in the film.

(4) The fracture mode of the Cu films seems to be a mixture of ductile and cleavage fracture. The contribution of brittle fracture increases with decreasing Cu film thickness. Films thinner than 70 nm show completely brittle fracture, indicating an increasing inherent brittleness of the Cu films.

ACKNOWLEDGMENTS

The synchrotron experiments were carried out at the MPI-MF Surface Diffraction beamline at ANKA (Forschungszentrum Karlsruhe, Germany). We thank A. Stierle, R. Weigel, and N. Kasper for excellent technical support. We like to extend our special thanks to F. Thiele, T. Wagner, and G. Richter of the MPI Thin Film Laboratory for the preparation of the thin films. We gratefully acknowledge S. Olliges and H.D. Carstanjen for performing the RBS measurements as well as M. Heinrich and S. Orso for their support in SEM work. We thank M.R. Begley and O.N. Scott for many suggestions and stimulating discussions.

REFERENCES

1. Y. Chen, J. Au, P. Kazlas, A. Ritenour, H. Gates, and M. McCreary: Flexible active-matrix electronic ink display. *Nature* **423,** 136 (2003).
2. G.H. Gelinck, H. Edzer, A. Huitema, E.V. Veenendaal, E. van Cantatore, L. Schrijnemakers, J. van der Putten, T.C.T. Geuns, M. Beenhakkers, J.B. Giesbers, B.H. Hiusman, E.J. Meijer, E.M. Benito, F.J. Touwslager, A.W. Marsman, B.J.E. van Rens, and D.M. De Leeuw: Flexible active-matrix displays and shift registers based on solution-processed organic transistors. *Nat. Mater.* **3,** 106 (2004).
3. E.R. Post, M. Orth, P.R. Russo, and N. Gershenfeld: E-broidery: Design and fabrication of textile-based computing. *IBM Syst. J.* **39,** 840 (2000).
4. E. Bonderover and S. Wagner: A woven inverter circuit for e-textile applications. *IEEE Electron Device Lett.* **25,** 295 (2004).
5. S. Wagner, S.P. Lacour, J. Jones, P.H.I. Hsu, J.C. Sturm, T. Li, and Z.G. Suo: Electronic skin: Architecture and components. *Physica E* **25,** 326 (2004).
6. J.U. Meyer: Retina implant—A bioMEMS challenge. *Sens. Actuators, A* **97-98,** 1 (2002).
7. A. Stett, U. Egert, E. Guenther, F. Hofmann, T. Meyer, W. Nisch, and H. Haemmerle: Biological application of microelectrode arrays in drug discovery and basic research. *Anal. Bioanal. Chem.* **377,** 486 (2003).
8. S. Zhang, D. Sun, Y.Q. Fu, and H.J. Du: Toughness measurement of thin films: A critical review. *Surf. Coat. Technol.* **198,** 74 (2005).
9. U.A. Handge, Y. Leterrier, G. Rochat, I.M. Sokolov, and A. Blumen: Two scaling domains in multiple cracking phenomena. *Phys. Rev. E: Stat. Phys., Plasmas, Fluids, Relat. Interdiscip. Topics* **62,** 7807 (2000).
10. G. Rochat, Y. Leterrier, P. Fayet, and J.A.E. Manson: Mechanical analysis of ultrathin oxide coatings on polymer substrates in situ in a scanning electron microscope. *Thin Solid Films* **437,** 204 (2003).
11. Y. Xiang, T. Li, Z.G. Suo, and J.J. Vlassak: High ductility of a metal film adherent on a polymer substrate. *Appl. Phys. Lett.* **87,** 61910 (2005).
12. M. Heinrich, P. Gruber, S. Orso, U.A. Handge, and R. Spolenak: Dimensional control of brittle nanoplatelets. A statistical analysis of a thin film cracking approach. *Nano Lett.* **6,** 2026 (2006).
13. U.A. Handge: Analysis of a shear-lag model with nonlinear elastic stress transfer for sequential cracking of polymer coatings. *J. Mater. Sci.* **37,** 4775 (2002).
14. Y. Leterrier, L. Boogh, J. Andersons, and J.A. Manson: Adhesion of silicon oxide layers on poly(ethylene terephthalate). I. Effect of substrate properties on coating's fragmentation process. *J. Polym. Sci., Part B: Polym. Phys.* **35,** 1449 (1997).
15. Y. Leterrier, J. Andersons, Y. Pitton, and J.A. Manson: Adhesion of silicon oxide layers on poly(ethylene terephthalate). II. Effect of coating thickness on adhesive and cohesive strengths. *J. Polym. Sci., Part B: Polym. Phys.* **35,** 1463 (1997).
16. N.E. Jansson, Y. Leterrier, and J.A.E. Manson: Modeling of multiple cracking and decohesion of a thin film on a polymer substrate. *Eng. Fract. Mech.* **73,** 2614 (2006).
17. N.E. Jansson, Y. Leterrier, L. Medico, and J.A.E. Manson: Calculation of adhesive and cohesive fracture toughness of a thin brittle coating on a polymer substrate. *Thin Solid Films* **515,** 2097 (2006).
18. B.E. Alaca, J.C. Selby, M.T.A. Saif, and H. Sehitoglu: Biaxial testing of nanoscale films on compliant substrates: Fatigue and fracture. *Rev. Sci. Instrum.* **73,** 2963 (2002).
19. Z. Chen and Z.H. Gan: Fracture toughness measurement of thin films on compliant substrate using controlled buckling test. *Thin Solid Films* **515,** 3305 (2007).
20. J. Böhm, P. Gruber, R. Spolenak, A. Stierle, A. Wanner, and E. Arzt: Tensile testing of ultrathin polycrystalline films: A synchrotron-based technique. *Rev. Sci. Instrum.* **75,** 1110 (2004).
21. P. Gruber, J. Böhm, A. Wanner, L. Sauter, R. Spolenak, and E. Arzt: Size effect on crack formation in Cu/Ta and Ta/Cu/Ta thin film systems, in *Nanoscale Materials and Modeling—Relations Among Processing, Mircostructure and Mechanical Properties*, edited by P.M. Anderson, T. Foecke, A. Misra, and R.E. Rudd (Mater. Res. Soc. Symp. Proc. **821,** Warrendale, PA, 2004), P2.7.

22. P. Gruber, J. Böhm, F. Onuseit, A. Wanner, R. Spolenak, and E. Arzt: Size effects on yield strength and strain hardening for ultra thin Cu films with and without passivation: A study by synchrotron and bulge test techniques. *Acta Mater.* **56,** 2318 (2008).
23. J.L. BeuthJr.: Cracking of thin bonded films in residual tension. *Int. J. Solids Struct.* **29,** 1657 (1992).
24. Z.C. Xia and J.W. Hutchinson: Crack patterns in thin films. *J. Mech. Phys. Solids* **48,** 1107 (2000).
25. J.L. Beuth and N.W. Klingbeil: Cracking of thin films bonded to elastic-plastic substrates. *J. Mech. Phys. Solids* **44,** 1411 (1996).
26. J.J. Vlassak: Channel cracking in thin films on substrates of finite thickness. *Int. J. Fract.* **119,** 299 (2003).
27. M.R. Begley and H. Bart-Smith: The electro-mechanical response of highly compliant substrates and thin stiff films with periodic cracks. *Int. J. Solids Struct.* **42,** 5259 (2005).
28. M.R. Begley, H. Bart-Smith, O.N. Scott, M.H. Jones, and M.L. Reed: The electro-mechanical response of elastomer membranes coated with ultra-thin metal electrodes. *J. Mech. Phys. Solids* **53,** 2557 (2005).
29. T. Li, Z.Y. Huang, Z. Suo, S.P. Lacour, and S. Wagner: Stretchability of thin metal films on elastomer substrates. *Appl. Phys. Lett.* **85,** 3435 (2004).
30. T. Li, Z.Y. Huang, Z.C. Xi, S.P. Lacour, S. Wagner, and Z. Suo: Delocalizing strain in a thin metal film on a polymer substrate. *Mech. Mater.* **37,** 261 (2005).
31. T. Li and Z. Suo: Deformability of thin metal films on elastomer substrates. *Int. J. Solids Struct.* **43,** 2351 (2006).
32. J. Dundurs and D.B. Bogy: Edge-bonded dissimilar orthogonal elastic wedges under normal and shear loading. *J. Appl. Mech.* **36,** 650 (1969).
33. R.W. Hertzberg: *Deformation and Fracture Mechanics of Engineering Materials* (John Wiley & Sons, NY, 1989), pp. 289–294.
34. K.J. Hsia, Z. Suo, and W. Yang: Cleavage due to dislocation confinement in layered materials. *J. Mech. Phys. Solids* **42,** 877 (1994).
35. N.R. Moody, D. Medlin, D. Boehme, and D.P. Norwood: Film thickness effects on the fracture of tantalum nitride on aluminum nitride thin film systems. *Eng. Fract. Mech.* **61,** 107 (1998).
36. P. Wellner, O. Kraft, G. Dehm, J. Andersons, and E. Arzt: Channel cracking of β-NiAl thin films on Si substrates. *Acta Mater.* **52,** 2325 (2004).